Chemistry Research Journal, 2025, 10(6):43-48
Available online www.chemrj.org

Research Article

ISSN: 2455-8990
CODEN(USA): CRJHA5

Photocatalytic Activity of Synthesized *Aegle marmelos* Leaf Nanoparticles of ZrO_2 Under UV And Visible Light

Abhilasha Bhatt*, Dr. Preeti Mehta, Dr. Pankaj Sen

Department of Chemistry, Sangam University Bhilwara Rajasthan, India

Abstract

Leaf-mediated synthesized ZrO_2 nanoparticles were evaluated for their photocatalytic activity in the degradation of effluent under UV and visible light irradiation. The study demonstrated that both pH and exposure time significantly influenced the degradation efficiency. Alkaline conditions (pH 9) showed superior photocatalytic performance, achieving up to 94% pollutant removal after 240 minutes, while acidic conditions (pH 3) exhibited lower efficiency. The enhanced activity is attributed to the generation of electron–hole pairs ($ZrO_2 + h\nu \rightarrow e^- + h^+$), which produce reactive hydroxyl (•OH) and superoxide ($\bullet O_2^-$) radicals responsible for oxidative degradation of contaminants. The results indicate that green-synthesized ZrO_2 nanoparticles are effective, sustainable photocatalysts for wastewater treatment, with potential applications in environmental remediation under both UV and visible light.

Keywords: ZrO_2 nanoparticles, Leaf-mediated synthesis, Photocatalysis, UV light, Visible light, Effluent degradation.

1. Introduction

***Aegle marmelos* (L.)** Corrêa, commonly known as bael, is an important medicinal tree of the family Rutaceae, widely distributed in India. Almost all parts of the plant—leaves, fruits, bark, and roots—are used in traditional medicine. The leaves are known for antidiabetic, anti-inflammatory, and antimicrobial properties, while the fruit pulp is valued for its digestive, antioxidant, and hepatoprotective activities. Phytochemical studies have reported the presence of alkaloids, flavonoids, coumarins, tannins, and essential oils, which contribute to its broad pharmacological potential. Nanotechnology is an interdisciplinary research domain that has gained considerable attention from scientists in physics, chemistry, biology, engineering, medicine, and materials science, owing to its ability to fabricate nanoparticles (NPs) with precisely controlled sizes and morphologies [1,2] Although numerous methods are available for the synthesis of nanoparticles, green synthesis approaches are increasingly favored because they are eco-friendly, economical, and sustainable compared to conventional physical and chemical techniques. Traditional chemical routes are often associated with high expenses and the use of toxic reagents [3,4], and they generally require stabilizing agents or additives to ensure nanoparticle stability.

In addition, such methods may involve non-biodegradable solvents and harsh reaction conditions, including elevated temperatures and high pressure [5–7]. Plant-derived phytochemicals play a crucial role in green nanoparticle synthesis by serving as natural reducing and capping agents. Various plant species, such as neem (*Azadirachta indica*), hibiscus (*Hibiscus rosa-sinensis*), Indian gooseberry (*Emblica officinalis*), and *Aegle marmelos*, have been effectively utilized for the synthesis of metal oxide nanoparticles. Among these, spinach is considered an efficient green source due to its abundance of vitamins (A, C, E, and K), folic and oxalic acids, and essential mineral

nutrients including Mn, Mg, Ca, P, Fe, Zn, Cu, Se, and K. Furthermore, spinach contains important bioactive compounds such as carotenoids (β-carotene, lutein, and zeaxanthin), chlorophyll, glutathione, α-lipoic acid, betaine, and diverse phenolic constituents, which collectively support nanoparticle formation, stabilization, and functional performance (8–11).

Direct exposure to dye-contaminated effluents poses severe risks to aquatic organisms, while in humans it has been associated with adverse effects ranging from skin irritation to serious illnesses such as cancer. Although various treatment strategies for dye-laden wastewater have been reported, continuous research is being undertaken to identify the most efficient and sustainable remediation approaches [12–15]. Recent investigations indicate that the textile sector consumes approximately 10–12% of the total dye production annually, including dyes such as Rhodamine B, Victoria blue, Rose Bengal, Indigo Red, Carmine, Red 120, Eriochrome, Methylene blue (MB), Crystal violet, and Methyl orange [16–19]. During manufacturing and application processes, nearly 20% of these dyes are released into wastewater streams. These colored contaminants are highly toxic, resistant to biodegradation, and harmful to living organisms [20,23]. Even at very low concentrations (below 1 ppm), dyes impart visible coloration to water bodies, leading to significant contamination of aquatic ecosystems. Consequently, the effective removal of dyes from industrial effluents is considered essential for environmental protection.

2. Material And Methods

Photocatalytic Degradation Methodology

(UV–Visible Assisted Photocatalytic Degradation; Modified Ahmad–Iravani Approach)

The photocatalytic experiments were performed using a combined visible–UV light irradiation system, following a modified protocol adapted from Ahmad et al. and Iravani, which are commonly employed for assessing dye degradation using metal oxide nanocatalysts [26], [27].

1. Preparation of Methylene Blue (MB) Solution

A stock solution of MB dye was prepared with deionized (DI) water. For each experimental run, a fresh working solution of 5 $mg \cdot L^{-1}$ MB was prepared in a 50 mL volume to maintain consistency in reaction conditions.

2. Catalyst Loading

A fixed amount of 150 mg of the synthesized ZrO_2 nanopowder was added to 50 mL of MB solution, corresponding to a catalyst concentration of 3 $g \cdot L^{-1}$. This dosage was selected based on prior optimization studies, which indicated effective radical generation, reduced electron-hole recombination, and minimal light scattering at this loading.

3. pH Optimization

To examine the effect of pH on photocatalytic efficiency, the MB solution was adjusted to pH 3, 7, and 9 using diluted HCl or NaOH. Measurements were taken with a calibrated digital pH meter. pH 7 was considered neutral, while pH 3 (acidic) and pH 9 (alkaline) were evaluated to investigate the influence of surface charge interactions on dye adsorption and subsequent degradation [198].

4. Irradiation Setup

Experiments were conducted in a borosilicate glass reactor placed beneath a 200 W visible light source. For UV-assisted experiments, a UV lamp of similar geometry was used. Continuous magnetic stirring ensured uniform dispersion of the catalyst and prevented sedimentation during irradiation.

5. Photocatalytic Reaction Procedure

Before light exposure, the MB–ZrO_2 suspension was stirred in the dark for 30 min to achieve adsorption–desorption equilibrium between the dye molecules and the nanoparticle surface. After dark equilibration, the reaction mixture was irradiated under visible or UV light for durations ranging from 60 to 250 min, depending on the experimental set.

6. Sampling and Analytical Measurements

Aliquots of 2–3 mL were withdrawn at 30 min intervals throughout the irradiation period. Each sample was immediately centrifuged to remove suspended catalyst particles. During the experiments, an aeration pump supplied a continuous oxygen flow to enhance the generation of reactive oxygen species and promote dye degradation. The clear supernatant was analyzed using a UV–Visible spectrophotometer at the characteristic absorption wavelength of

MB ($\lambda_{max} \approx 664$ nm). Degradation efficiency (%) was determined based on the reduction in absorbance relative to the initial concentration.

7. Kinetic Analysis

The photocatalytic degradation kinetics were evaluated using the pseudo-first-order model to describe the reaction rate and assess the efficiency of the ZrO_2 nanoparticles under UV and visible light irradiation.

3. Result and Discussion

Table 1: Effluent Treatment Under UV Light Using Leaf-Mediated Synthesised ZrO_2 Nanoparticles ($ZrOCl_2 \cdot 8H_2O$)

Time (min)	Degradation Efficiency (%) at pH 3	Degradation Efficiency (%) at pH 7	Degradation Efficiency (%) at pH 9
30	12	22	38
60	31	22	38
90	49	31	52
120	63	45	67
150	78	52	74
180	86	58	81
210	91	63	87
240	94	68	92

The photocatalytic performance of leaf-mediated synthesized ZrO_2 nanoparticles under UV irradiation showed a clear dependence on reaction time and pH conditions. As presented in Table, degradation efficiency increased progressively with exposure time at all pH levels. At pH 3, the degradation rate rose from 12% after 30 minutes to 94% at 240 minutes. Under neutral conditions (pH 7), the efficiency improved from 22% to 68% over the same duration. Notably, alkaline conditions (pH 9) exhibited superior photocatalytic activity, achieving 38% degradation at 30 minutes and reaching 92% after 240 minutes. The enhanced performance at higher pH may be attributed to increased generation of reactive hydroxyl radicals, which facilitate faster breakdown of effluent contaminants. Overall, the results indicate that alkaline pH and prolonged irradiation significantly enhance the photocatalytic efficiency of ZrO_2 nanoparticles under UV light.

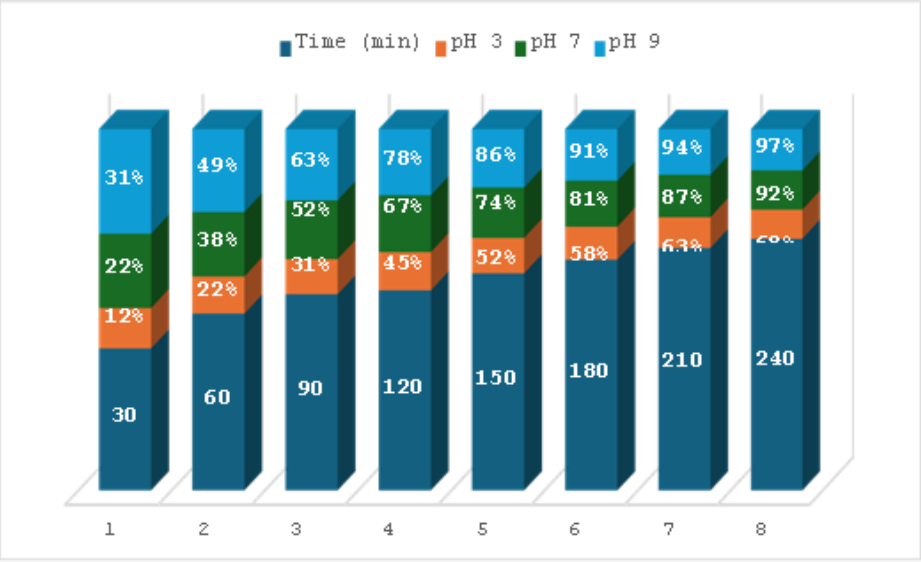


Figure 1: Graphical Representation of Effluent Treatment Under UV Light Using Leaf-Mediated Synthesised ZrO_2 Nanoparticles ($ZrOCl_2 \cdot 8H_2O$) TIME / pH

Table 2: Effluent Treatment Under Visible Light Using Leaf- Mediated Synthesised ZrO_2 Nanoparticles ($ZrOCl_2 \cdot 8H_2O$) Time / pH

Time (min)	pH 3	pH 7	pH 9
30	10%	14%	18%
60	18%	24%	31%
90	25%	34%	42%
120	36%	50%	62%
150	42%	58%	71%
180	48%	66%	78%
210	57%	81%	90%
240	63%	89%	94%

The photocatalytic degradation of effluent using leaf-mediated ZrO_2 nanoparticles under visible light increased with time and pH. Maximum removal (94%) was observed at pH 9 after 240 min, while acidic conditions (pH 3) showed only 63% degradation. Higher pH favors enhanced formation of reactive species. Upon irradiation, ZrO_2 generates electron–hole pairs ($ZrO_2 + h\nu \rightarrow e^- + h^+$), where holes produce hydroxyl radicals ($h^+ + H_2O/OH^- \rightarrow \bullet OH$) and electrons reduce oxygen to superoxide radicals ($e^- + O_2 \rightarrow \bullet O_2^-$). These radicals oxidize pollutants to CO_2, H_2O, and inorganic ions, explaining the improved photocatalytic efficiency under alkaline conditions.

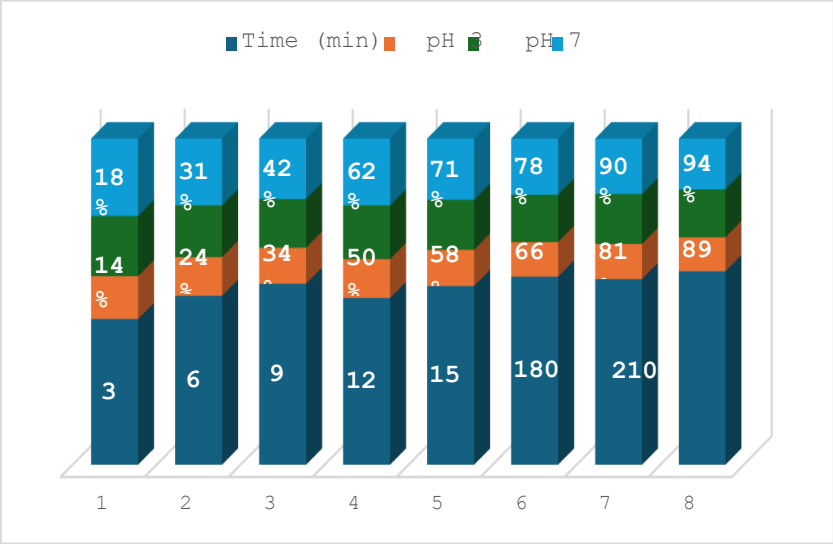


Figure 2: Graphical Representation of Effluent Treatment Under Visible Light Using Leaf-Mediated Synthesised ZrO_2 Nanoparticles ($ZrOCl_2 \cdot 8H_2O$) Time / pH

4. Discussion

The photocatalytic performance of leaf-mediated ZrO_2 nanoparticles is significantly influenced by both pH and irradiation time. Alkaline conditions (pH 9) consistently demonstrated higher degradation efficiency, likely due to the increased availability of hydroxide ions that facilitate the formation of highly reactive hydroxyl radicals (•OH). The generation of electron–hole pairs under visible or UV light ($ZrO_2 + h\nu \rightarrow e^- + h^+$) triggers the production of •OH and superoxide radicals ($\bullet O_2^-$), which oxidize organic pollutants into CO_2, H_2O, and simpler inorganic ions. Prolonged irradiation enhances radical production and ensures complete degradation of effluent contaminants. The comparatively lower efficiency at acidic and neutral pH suggests limited radical generation and less effective charge separation under these conditions. These findings underscore the importance of pH optimization in maximizing the photocatalytic efficiency of ZrO_2 nanoparticles.

5. Conclusion

Leaf-mediated ZrO_2 nanoparticles exhibit excellent photocatalytic activity for effluent degradation under visible and UV light. Maximum efficiency is achieved at alkaline pH with extended irradiation, highlighting the role of reactive species generated through electron–hole pair formation. The study demonstrates the potential of green-synthesized ZrO_2 nanoparticles as an effective, sustainable, and environmentally friendly approach for wastewater treatment, offering a promising alternative to conventional methods.

Reference

[1]. Ahmed KA, Huang K. Formation of Mn3O4nanobelts through the solvothermal process and their photocatalytic property. Arab J Chem. 2019; 12(3):429-439. https://doi.org/10.1016/j.arabjc.2014.08.014

[2]. Bello A, Fashedemi OO, Lekitima JN, Fabiane M, Dodoo-Arhin D, Ozoemena KI, GogotsiY, Charlie Johnson AT, Manyala N. High-performance symmetric electrochemical capacitor based on graphene foam and nanostructured manganese oxide. AIP Advances. 2013; (8): 082118.https://doi.org/10.1063/1.4819270

[3]. Hafez AA, Naserzadeh P, Ashtari K, Mortazavian AM, Salimi A. Protection of manganese oxide nanoparticles-induced liver and kidney damage by vitamin D. RTP. 2018; 98:240-244. https://doi.org/10.1016/j.yrtph.2018.08.005

[4]. Abduljabar MA, Merza SH. Graphene oxide decorated with nickel cobaltite nanoparticles as an adsorbent for cationic methyl green dye: Kinetic, isotherm, and thermodynamic studies. Baghdad Sci J. 2024; 21(9):2853. https://doi.org/10.21123/bsj.2024.8742.

[5]. Ahmad KS, Yaqoob S, Gul MM. Dynamic green synthesis of iron oxide and manganese oxide nanoparticles and their cogent antimicrobial, environmental and electrical applications. Rev Inorg Chem. 2022; 42(3):239-263.https://doi.org/10.1515/revic-2021-0033.

[6]. Perachiselvi M, Bagavathy MS, Samraj JJ, Pushpalaksmi E, Annadurai G. Synthesis and characterization of Mn3O4nanoparticles for biological studies. Appl Ecol Environ Sci. 2020; 8(5):273-277. https://doi.org/10.12691/aees-8-5-13.

[7]. Fatin A. Al-jubouri, Basim I. Al-Abdaly. Anti-oxidant and anti-microbial activities of [ZnO: CoO/ Eugenol]and [ZnO:Fe2O3/Eugenol] nanocomposites. IHJPAS. 2024; 37(1):251-64.https://jih.uobaghdad.edu.iq/index.php/j/article/view/3233.

[8]. Jiménez-Pérez ZE, Singh P, Kim YJ, Mathiyalagan R, Kim DH, Lee MH, Yang DC. Applications of Panax ginseng leaves-mediated gold nanoparticles in cosmetics relation to antioxidant, moisture retention, and whitening effect on B16BL6 cells. J Ginseng Res. 2018; 42(3):327-333.https://doi.org/10.1016/j.jgr.2017.04.003.

[9]. Khan S, Ansari AA, Khan AA, Abdulla M, Al-Obeed O, Ahmad R. In vitro evaluation of anticancer and biological activities of synthesized manganese oxide nanoparticles. Med Chem Comm. 2016; 7(8): 1647-1653.https://doi.org/10.1039/C6MD00219F.

[10]. Alagarsamy A, Chandrasekaran S, Manikandan A. Green synthesis and characterization studies of biogenic zirconium oxide (ZrO2) nanoparticles for adsorptive removal of methylene blue dye. J Mol Struct. 2022; 1247:131275. https://doi.org/10.1016/j.molstruc.2021.131275

[11]. Vijayakumar A, Chacko A, Jayaprakash P. Green synthesis of Mn3O4nanoparticles in zinc chloride: Urea: acetamide deep eutectic solvent-characterization, fluorescence sensing, antibacterial and antioxidant properties. JMol Struct. 2025; 1321:139833. https://doi.org/10.1016/j.molstruc.2024.139833.

[12]. Samsami, S.; Mohamadizaniani, M.; Sarrafzadeh, M.H.; Rene, E.R.; Firoozbahr, M. Recent advances in the treatment of dye-containing wastewater from textile industries: Overview and perspectives. Process. Saf. Environ. Prot. 2020, 143, 138–163. [Google Scholar] [CrossRef]

[13]. Sivagami, M.; Asharani, I.V. Phyto-mediated Ni/NiO NPs and their catalytic applications—A short review. Inorg. Chem. Commun. 2022, 145, 110054. [Google Scholar] [CrossRef]

[14]. Ravichandran, S.; Thangaraj, P.; Sengodan, P.; Radhakrishnan, J. Biomimetic facile synthesis of cerium oxide nanoparticles for enhanced degradation of textile wastewater and phytotoxicity evaluation. Inorg. Chem. Commun. 2022, 146, 110037. [Google Scholar] [CrossRef]

[15]. Younis, A.M.; Alminderej, F.M.; Alluhayb, A.H.; Saleh, S.M.; Aissa, M.A.B.; Modwi, A. Synergistic adsorption of methylene blue from aqueous medium using MgO-Y2O3@ gC3N4 (MYCN) nanocomposite: Performance evaluation and kinetic study. Nano-Struct. Nano-Objects 2024, 39, 101267. [Google Scholar] [CrossRef]

[16]. Katowah, D.F.; Saleh, S.M.; Mohammed, G.I.; Alkayal, N.S.; Ali, R.; Hussein, M.A. Ultra-efficient hybrid material-based cross-linked PANI@Cs-GO-OXS/CuO for the photocatalytic degradation of Rhodamine-B. J. Phys. Chem. Solids 2021, 157, 110208. [Google Scholar] [CrossRef]

[17]. Alharbi, F.K.; Albadri, A.E.; Modwi, A.; Saleh, S.M. Effectiveness of Ag@NiO@g-C3N4 photocatalysts: Green fabrication and superior photocatalysis capability. Opt. Mater. 2024, 152, 115410. [Google Scholar] [CrossRef]

[18]. Katowah, D.F.; Saleh, S.M.; Alqarni, S.A.; Ali, R.; Mohammed, G.I.; Hussein, M.A. Network structure-based decorated CPA@CuO hybrid nanocomposite for methyl orange environmental remediation. Sci. Rep. 2021, 11, 5056. [Google Scholar]

[19]. Ben Aissa, M.A.; Modwi, A.; Albadri, A.E.; Saleh, S.M. Dependency of crystal violet dye removal behaviors onto mesoporous V2O5-g-C3N4 constructed by simplistic ultrasonic method. Inorganics 2023, 11, 146. [Google Scholar] [CrossRef]

[20]. Weldegebrieal, G.K. Synthesis method, antibacterial and photocatalytic activity of ZnO nanoparticles for azo dyes in wastewater treatment: A review. Inorg. Chem. Commun. 2020, 120, 108140. [Google Scholar] [CrossRef]

[21]. Mehra, S.; Singh, M.; Chadha, P. Adverse impact of textile dyes on the aquatic environment as well as on human beings. Toxicol. Int. 2021, 28, 165. [Google Scholar] [CrossRef]

[22]. T. Ahmad et al., "Photocatalytic degradation of organic dyes using green-synthesized metal oxide nanoparticles: mechanism and kinetics," Environ. Sci. Pollut. Res., vol. xx, pp. xx–xx, 2021.

[23]. S. Iravani, "Green synthesis of metal nanoparticles using plants," Green Chem., vol. 13, no. 10, pp. 2638–2650, 2011.SpringerLink